Epilepsy & Behavior 139 (2023) 109072

Contents lists available at ScienceDirect

Epilepsy & Behavior

journal homepage: www.elsevier.com/locate/yebeh

Intermittency properties in a temporal lobe epilepsy model

F.S. Borges [a,b,*], E.C. Gabrick [c], P.R. Protachevicz [d], G.S.V. Higa [b,e], E.L. Lameu [f], P.X.R. Rodriguez [b,g], M.S.A. Ferraz [b], J.D. Szezech Jr. [c,h], A.M. Batista [c,d,h], A.H. Kihara [b,*]

[a] Department of Physiology and Pharmacology, State University of New York Downstate Health Sciences University, Brooklyn, NY, USA
[b] Center for Mathematics, Computation, and Cognition, Federal University of ABC, São Bernardo do Campo, SP, Brazil
[c] Graduate in Science Program - Physics, State University of Ponta Grossa, Ponta Grossa, PR, Brazil
[d] Institute of Physics, University of São Paulo, São Paulo, SP, Brazil
[e] Institute of Chemistry, University of São Paulo, São Paulo, SP, Brazil
[f] Snyder Institute for Chronic Diseases, University of Calgary, Calgary, AB, Canada
[g] Faculty of Medicine, University of Bonn, Bonn, Germany
[h] Department of Mathematics and Statistics, State University of Ponta Grossa, Ponta Grossa, PR, Brazil

ARTICLE INFO

Article history:
Received 5 October 2022
Revised 22 December 2022
Accepted 26 December 2022
Available online 16 January 2023

Keywords:
Synchronization
Epileptogenesis
Network
Optogenetics
Seizures
Epilepsy biomarker

ABSTRACT

Neuronal synchronization is important for communication between brain regions and plays a key role in learning. However, changes in connectivity can lead to hyper-synchronized states related to epileptic seizures that occur intermittently with asynchronous states. The activity-regulated cytoskeleton-associated protein (ARC) is related to synaptic alterations which can lead to epilepsy. Induction of status epilepticus in rodent models causes the appearance of intense ARC immunoreactive neurons (IAINs), which present a higher number of connections and conductance intensity than non-IAINs. This alteration might contribute to abnormal epileptic seizure activity. In this work, we investigated how IAINs connectivity influences the firing pattern and synchronization in neural networks. Firstly, we showed the appearance of synchronized burst patterns due to the emergence of IAINs. Second, we described how the increase of IAINs connectivity favors the appearance of intermittent up and down activities associated with synchronous bursts and asynchronous spikes, respectively. Once the intermittent activity was properly characterized, we applied the optogenetics control of the high synchronous activities in the intermittent regime. To do this, we considered that 1% of neurons were transfected and became photosensitive. We observed that optogenetics methods to control synchronized burst patterns are effective when IAINs are chosen as photosensitive, but not effective in non-IAINs. Therefore, our analyses suggest that IAINs play a pivotal role in both the generation and suppression of highly synchronized activities.

1. Introduction

According to International League Against Epilepsy (ILAE), a seizure is a transient state characterized by abnormal excessive or synchronous activity in the brain [1]. Although seizure activity can occur in different time scales, there is not a minimum time characterized so far [2]. For instance, the duration of an absence seizure is in the time range of 3 to 30 s [3]. Tonic seizures are typically less than 15 s, although they can reach up to 1 min [4]. In turn, generalized tonic–clonic seizures commonly are not longer than 2-3 min [5]. Also, status epileptic, an extreme epileptic activity, can persist over 5 min [6,7]. Jenssen et al. [8] highlighted the necessity of new studies about long seizures to improve treatments. Several studies indicated that epileptic activity emerges from modifications in the neuronal network [9–11]. Borges et al. [12] determined that spike-to-burst activity emerges in a neuronal model with excitability adaptation and a high excitatory synaptic conductance. Also, Kinjo et al. [13] reported that the degree of connections plays an essential role in neuronal activity control. Besides that, Morgan and Soltesz demonstrated that high-interconnected-excitatory neurons, denominated "hub neurons", strongly influence the activity in the hippocampal neuronal network, increasing its excitability [14].

Network modifications are triggered by distinct mechanisms that regulate synaptic plasticity [15]. Janz et al. [17] reported that excessive synapses in the excitatory neurons of the hippocampus

* Corresponding authors at: Department of Physiology and Pharmacology, State University of New York Downstate Health Sciences University, Brooklyn, NY, USA (F.S. Borges); Center for Mathematics, Computation, and Cognition, Federal University of ABC, São Bernardo do Campo, SP, Brazil (A.H. Kihara).
E-mail addresses: fernandodasilvaborges@gmail.com (F.S. Borges), alexandrekihara@gmail.com (A.H. Kihara).

https://doi.org/10.1016/j.yebeh.2022.109072
1525-5050/

contribute to epileptic activity. In this context, activity-regulated cytoskeleton-associated protein (ARC), also known as Arc/Arg3.1 or Arg3.1, assumes a pivotal role by promoting network reorganization, due to its participation in synaptic plasticity [18,19]. Indeed, ARC might participate in synaptic alterations which can lead to epilepsy [20]. High ARC expression in excitatory neurons is correlated with persistent firing patterns due to an increase in the number of excitatory connections in specific cortical neuronal populations [21]. Interestingly, it was reported that even a small number of excitatory highly-connected neurons are able to increase excitability and create potential epileptic circuits [14]. Also, the severity and frequency of epileptic discharges have been associated with aberrant integration of excitatory neurons originated by hippocampal neurogenesis in animal models of temporal lobe epilepsy (TLE) [22]. Although high ARC expression has been largely observed in excitatory neurons, in inhibitory interneurons it is less expressed [23]. Several aspects underlie the establishment of an epileptic network, including changes in synaptic inputs and neuronal biophysical properties [24]. Despite the great number of studies related to network changes in epilepsy, several questions remain unsolved. Therefore, there is an effort to understand how the epileptic networks establish an intermittent state, comprising the shift between a balanced network of events to a hyperexcitable and hyper synchronized network of events [25].

Hauptmann et al. [26] discuss how burst intermittent patterns can be related to epileptic activities in a neuronal network model. Koronovskii et al. [27] showed that the time distribution of spike-wave discharges and sleep spindles in epileptic brains exhibit two types of intermittent behavior alternating over time. The theoretical statistic proposed by them agrees with experimental intermittent power-law distributions observed on WAG/Rij rats [27]. Other work-related phenomenon of intermittent phase synchronization to the epileptic activities [28]. Moreover, phase synchronization has been associated with seizure termination [29]. Moskalenko et al. [30] proposed a method to estimate intermittent phase synchronization in the human epileptic brain using the Lyapunov exponent.

The optogenetics methodology allows precise control of neuron functions using optics, genetics, and bioengineering [31], which support the investigation of distinct neuronal network mechanisms including in epilepsy [32]. By expressing an exogenous photo-sensitive channel, neurons become responsive to light and their dynamics can be controlled [33]. Optogenetics provides an excitability-neuronal control by different frequencies of light [34]. Channelrhodopsin-2 and Halorhodopsin are two common light-sensitive channels used to excite and inhibit neurons, respectively. Channelrhodopsin-2 is activated by blue light causing excitation, while Halorhodopsin is activated with yellow light causing neuronal inhibition [35]. Light emission is capable of reducing high synchronous activities and avoids epileptiform activities [36]. The inhibition of excitatory and inhibitory cells by optogenetics was considered to control spontaneous seizures in temporal lobe epilepsy [37]. In neocortical drug-resistant epilepsy, the optogenetics inhibition of some neurons were capable of reducing seizures [38]. Although more studies are necessary, the optogenetics approach is a promising treatment for epilepsy [39].

In this work, using immunofluorescence analyzes of ARC in coronal sections of the hippocampus, we observed that intense ARC immunoreactive neurons (IAINs) appear in the rat hippocampus after status epilepticus. To understand the effect of network alteration in brain activity, we proposed a random neuronal network model [40] composed of excitatory and inhibitory adaptive exponential integrate-and-fire neurons (AdEx) [41]. Networks of the AdEx model have been shown to be efficient to describe characteristics of epileptic burst synchronization in the brain [12,10,49], as well as asynchronous firing patterns [42,43]. First, we modeled a nonepileptic network (control), characterized by an asynchronous activity [44,45], where all neurons have the same probability and strength of the connection. Then, we randomly selected a fraction of excitatory neurons to increase their afferent probability connection and/or synaptic strength, making them behave as "hub" (stronger and/or highly connected) neurons, such as observed in high-expressed ARC neurons. For this reason, the selected neurons were called IAINs (intense ARC immunoreactive neurons).

Our numerical simulations indicated that increasing afferent probability or synaptic strength has the same effect on the random network model. In both cases, we observed an intermittent-firing-pattern behavior between asynchronous rhythm and burst-synchronization pattern. As the strength of IAIN connections increases, hyper-synchronized burst events emerge. Initially, the duration of most hyper-synchronous events (τ) is less than 10 s, and the distribution of these τ can be fitted in a power law. Therefore, this may represent a mild-to-moderate state of epilepsy, where most seizures are local. When the strength of connections to IAINs is even greater, the frequency and duration of hyper-synchronization events increase, lasting longer than tens of minutes. Moreover, the τ distribution of fewer than 10 s events follows a power-law distribution, and longer events are best fitted by exponential distributions. These long seizures are usually generalized and related to severe epilepsy that is fatal if not treated effectively [16]. Finally, we proposed a model based on optogenetics for seizure control targeting IAIN cells. Application of light stimuli to 10% of ARC cells for 3 s proved to be effective for silencing seizures (hyper synchronization). When the same stimulus was applied randomly to the same number of neurons, it did not interrupt the hyper-synchronization activity. Therefore, our model demonstrates that intense ARC immunoreactive neurons (IAINs) may have the potential to control epileptic seizures.

Our work is organized as follows: In Section 2, we presented the methodology of the animal model and numerical simulations. Section 3, shows our results of epileptic pattern simulations as well as the optogenetics approach to suppress the high neuronal synchronization. In the last section, we draw our conclusions.

2. Methodology

2.1. ARC in the epileptogenesis

Several experimental evidences show that seizure induction promotes neuronal up-regulation of ARC expression in the hippocampus [17,46]. However, the distribution pattern and the characteristics of this expressing ARC cells during epileptogenesis have not been characterized so far. In order to clarify this, pilocarpine-induced status epilepticus (SE) was performed in male adult Wistar rats (*Rattus norvegicus*). ARC immunolabeling was analyzed 48 h after SE interruption in the hippocampal region. The results of the control and after-status epilepticus (ASE) groups were compared. The most evident change observed in the experimental hippocampi was the emergence of intense ARC immunoreactive neurons (IAINs) in the ASE group.

Fig. 1 shows the CA1 region of a representative control hippocampus (Fig. 1(a)), and of an after-status epilepticus (ASE) group, where the appearance of IAINs was observed (Fig. 1(b)). These neurons shared features of high immunoreactivity for ARC in the cytosol, neurites, and the nucleus. To evaluate whether the IAINs observed in the ASE period represent a different neuronal population regarding ARC expression, we calculated the probability density distribution of ARC intensity of control and ASE animals using a method known as Kernel Density Estimation [47]. Then, the density probability distribution of each region was fitted using

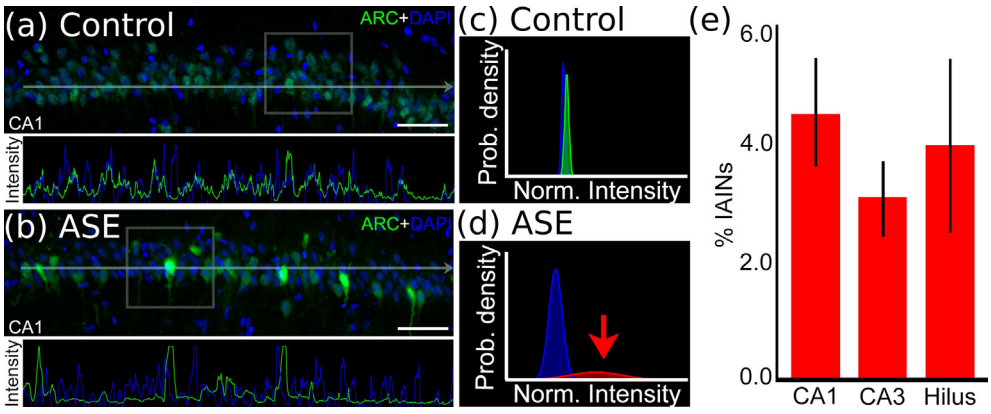

Fig. 1. Characterization of intense ARC immunoreactive neurons (IAINs) in the rat hippocampus after status epilepticus (ASE). Immunofluorescence analyses of ARC (green) in coronal sections of hippocampi from controls and ASE animals counterstained with DAPI (blue). (a) In the representative image of CA1, where we did not detect IAINs. (b) In CA1 of ASE animals, we observed a high accumulation of ARC in the cytosol, processes, and especially in the nucleus in some neurons, as confirmed by the pixel intensity profile. (c, d) Probability density distributions of ARC intensity in CA1 region of control and ASE group, respectively. The probability density distributions were fitted using two Gaussians to identify different types of cells regarding their accumulation of ARC. Note that in the control group, there is an overlap of both Gaussians, while in the ASE group, this overlap is absent, indicating that there are two populations of neurons regarding the intensity of ARC staining in the experimental group. The same analysis was performed for the CA3 and the hilus. (e) The proportion of IAINs relative to the total number of neurons in CA1, CA3, and hilus of the experimental hippocampus. Bars represent standard errors of the mean. Scale bars: 50 μm (a, b).

Gaussian curves to identify different groups of cells regarding their pixel intensity. Fig. 1(c) shows an overlap between both Gaussians in CA1 of the control group, indicating the presence of just one neuronal population regarding ARC expression. In contrast, in CA1 of the ASE group, we did not observe an overlap of the curves (Fig. 1(d)). In this case, the red curve (red arrow) is distributed over higher pixel intensity values with lower probability density and may represent the IAIN population that appears in CA1 only in ASE animals. A similar pattern was observed in CA3 and in the hilus. These results indicated the appearance of a new neuronal population regarding ARC protein accumulation in CA1, CA3, and in the hilus during the ASE period of the pilocarpine model of TLE, in agreement with our morphological observations of IAINs in these areas. Finally, we determined the proportion of this neuronal population in the hippocampus. The mean point of intersection between the Gaussian curves in CA1, CA3, and hilus (1.95 ± 0.11, normalized intensity) of the experimental group was used as a threshold to quantify the number of IAINs in each region. These analyses showed that IAINs represent 4.73% ± 0.91 of the entire neuronal population in CA1, 3.26% ± 0.61 in CA3 and 4.18% ± 1.46 in the hilus (Fig. 1(e)). These results are also consistent with our mathematical approach, where the probabilities of appearance for IAINs were low in experimental animals.

2.2. Network model

We constructed a random neuronal network [40] composed of N = 1000 neurons where 80% were excitatory and 20% inhibitory, connected by chemical synapses. This neural population ratio together with the consideration that synaptic conductance is 4 times greater for inhibitory than excitatory synapses, represents the balance between excitation and inhibition in our hippocampus model. This network reproduces some hippocampal activities observed *in vitro* [42] and *in vivo* [48]. We do not create self-connections for both excitatory and inhibitory neurons [49,50]. The excitatory neurons were subdivided into two types: IAIN and non-IAIN. The fraction of IAINs in the excitatory network was identified by the parameter f_{IAIN}. Fig. 2 shows a schematic representation of connection in the considered neuronal network. Fig. 2(a) shows excitatory non-IAINs (red triangles) and IAINs (brown triangles), as well as the inhibitory ones (blue circles) in the neuronal network. Excitatory and inhibitory connections are represented by red and blue lines, respectively. The intensity of each connection is proportional to the line thickness. Fig. 2(b-d) highlights the differences between non-IAINs and IAINs. Fig. 2(b) shows an excitatory non-IAIN with a typical connection probability p and excitatory conductance g_{exc}. Note that in this case, the amount and the intensity of connections are relatively small and weaker than in Fig. 2(c) and 2(d), respectively. In Fig. 2(c), it is represented by an increase in afferent synapse number, where the relative proportion of afferent synapse numbers between IAINs and non-IAIN (n_{IAIN}) cells is greater than one. Fig. 2(d) shows an increase in the

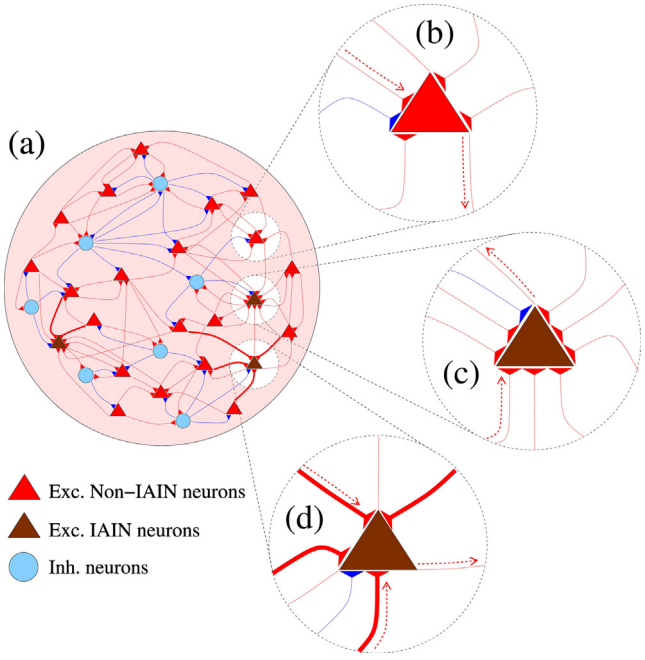

Fig. 2. (a) Schematic representation of the neuronal network composed of excitatory non-IAINs (red triangles), excitatory IAINs (brown triangles), and inhibitory neurons (blue circles). (b) Typical excitatory connection probability (p) arriving at a non-IAIN excitatory neuron. (c) Augmented excitatory connections probability in an IAIN excitatory neuron associated with the n_{IAIN} parameter. (d) Increased the excitatory synaptic strength arriving on an IAIN excitatory neuron associated with the g_{IAIN} parameter.

synaptic conductance arriving on IAINs. This increase is associated with the IAIN relative conductance intensity ($g_{\mathrm{IAIN}} \geqslant 1$) in the mathematical model.

2.3. Neuron dynamics

The membrane potential of each neuron was described by the adaptive exponential integrate-and-fire model that consists of a two differential equations system [41,51]. The correspondent dynamics and synaptic transmission of each neuron i in the network is given by

$$\begin{aligned} C\frac{dV_i}{dt} = & -g_{\mathrm{L}}(V_i - E_{\mathrm{L}}) + g_{\mathrm{L}}\Delta_{\mathrm{T}}\exp\left(\frac{V_i - V_{\mathrm{T}}}{\Delta_{\mathrm{T}}}\right) \\ & -w_i + I + \sum_{k=1}^{N}\left(V_{\mathrm{rev}}^{k} - V_i\right)A_{ik}g_k \quad (1) \\ \tau_{\mathrm{w}}\frac{dw_i}{dt} = & \; a(V_i - E_{\mathrm{L}}) - w_i, \\ \tau_{\mathrm{s}}\frac{dg_i}{dt} = & -g_i, \end{aligned}$$

where V_i is the membrane potential, w_i is the adaptation current, and g_i is the synaptic conductance of each neuron i. C parameter represents neuronal capacitance. g_{L} and E_{L} correspond to the leak conductance and reversal potential, respectively. I and V_{T} correspond to the current applied and the threshold potential, respectively. The parameter Δ_{T} controls the sharpness of the initial phase of the spike [52] and in the limit $\Delta_{\mathrm{T}} \to 0$ the neuron model becomes the adaptive integrate-and-fire model [53]. The synaptic reversal potentials and conductances depend on the type of chemical connection. V_{rev}^{k} assume $V_{\mathrm{rev}}^{\mathrm{ex}}$ value for excitatory connections and $V_{\mathrm{rev}}^{\mathrm{in}}$ for inhibitory ones. g_k is the synaptic conductance from the presynaptic neuron k. A_{ik} represents the adjacency matrix where 1 value elements indicate that there is a connection from k to i while 0 value represents the absence of such connection. a and τ_{s} represent the sub-threshold adaptation intensity and adaptation time decay, respectively. In this model, if $V_i(t)$ reaches to a peak potential V_{peak}, a reset condition is applied

$$V_i \to V_{\mathrm{r}}, \quad (2)$$

$$w_i \to w_{\mathrm{r}} = w_i + b, \quad (3)$$

$$g_i \to g_i + g_{\mathrm{s}}. \quad (4)$$

In the first, V_{r} represents the reset potential. In the second, b indicates the value of spike-triggered adaptation current. In the last, g_{s} assume value g_{ex} for afferent excitatory synapses in non-IAINs, $g_{\mathrm{IAIN}}^{\mathrm{ex}} = g_{\mathrm{IAIN}} \times g_{\mathrm{ex}}$ for IAINs afferent excitatory synapses, and g_{in} for inhibitory connections. All numerical simulations were implemented in C and we considered the Fourth Order Runge–Kutta integration method with a time step equal to δt = 0.01 ms. Table 1 shows the standard neuronal parameters considered in the simulations.

2.4. Diagnostics

To identify spiking and bursting firing patterns, we utilize the mean coefficient of variation (CV) of the neuronal inter-spike interval (ISI), which is given by

$$\overline{\mathrm{CV}} = \frac{\sigma_{\mathrm{ISI}}}{\overline{\mathrm{ISI}}}, \quad (5)$$

where σ_{ISI} is the standard deviation of the ISI normalized by the mean $\overline{\mathrm{ISI}}$ [54,55], both σ_{ISI} and $\overline{\mathrm{ISI}}$ were calculated over all neuron spikes. In the considered model, spiking patterns produces $\overline{\mathrm{CV}} < 0.5$ while bursting ones $\overline{\mathrm{CV}} \geqslant 0.5$ [10,12]. As the patterns of spikes and bursts of intermittent behavior change over time, for this reason, an instantaneous coefficient of variation $\mathrm{CV}(t)$ was also calculated, where for each time t, 4 ISIs before and 4 after time t were used in the calculation.

Table 1
Standard neuronal parameters.

Symbol	Description	Value
N	Number of neurons	1000
p	Connection probability	0.1
f_{IAIN}	Fraction of IAIN neurons	[0,0.2]
n_{IAIN}	Ratio of IAIN and non-IAIN afferent synapse number	[1.0,1.4]
C	Neuronal capacitance	200 pF
g_{L}	Leak conductance	12 nS
E_{L}	Leak reversal potential	−70 mV
Δ_{T}	Slope factor	2 mV
V_{T}	Threshold potential	−50 mV
I	Constant current	512.4 pA
$V_{\mathrm{rev}}^{\mathrm{ex}}$	Excitatory reversal potential	0 mV
$V_{\mathrm{rev}}^{\mathrm{in}}$	Inhibitory reversal potential	−80 mV
V_{peak}	Peak potential	0 mV
V_{r}	Reset potential	−58 mV
τ_{w}	Adaptation time constant	300 ms
a	Sub-threshold adaptation	2 nS
b	Triggered adaptation	70 pA
τ_{s}	Synaptic time constant	2.728 ms
g_{in}	Inh. conductance	2.0 nS
g_{ex}	Exc. non-IAIN conductance	0.5 nS
g_{IAIN}	Ratio IAIN conductance	[1.0,2.0]
$g_{\mathrm{IAIN}}^{\mathrm{ex}}$	Exc. IAIN conductance	[0.5,1.0] nS
δt	Integration time step	10^{-2} ms

To determine synchronous behavior, we considered the complex phase order parameter [56] defined as

$$\mathrm{R(t)} = \left|\frac{1}{\mathrm{N}}\sum_{\mathrm{i}=1}^{\mathrm{N}}\exp(\mathrm{j}\psi_{\mathrm{i}})\right|, \quad (6)$$

where $\mathrm{j}=\sqrt{-1}$, and the phase of each neuron i is given by

$$\psi_i(t) = 2\pi m + 2\pi\frac{t - t_i^m}{t_i^{m+1} - t_i^m}. \quad (7)$$

t_i^m corresponds to the time when a spike m ($m = 0, 1, 2, \ldots$) of a neuron i happens ($t_i^m < t < t_i^{m+1}$). We have considered the beginning of the spike when $V_i > 0$ mV. The value of the order parameter goes to 1 in a totally synchronized state and 0 for totally asynchronized ones. To study the neuronal synchronization of the network, we have calculated the time-average order parameter, which is given by

$$\overline{R} = \frac{1}{t_{\mathrm{fin}} - t_{\mathrm{ini}}}\sum_{t_{\mathrm{ini}}}^{t_{\mathrm{fin}}} R(t), \quad (8)$$

where $t_{\mathrm{fin}} - t_{\mathrm{ini}}$ is the time window for calculating $\overline{R}$. The burst synchronization is observed when $\mathrm{CV}(t) \geqslant 0.5$ and $\overline{R} \geqslant 0.5$.

2.5. Experimental procedures in the animal model

The experiments were performed using male adult Wistar rats (Rattus norvegicus) weighing 290 g-320 g maintained under controlled temperature (20°-22°C) with a 12-h dark/light cycle at the vivarium of Universidade Federal do ABC in São Bernardo do Campo-SP with free access to food and water. All experimental procedures were performed under the Ethics Committee for Animal Experimentation of Universidade Federal do ABC (Protocol No. 013/2014). Animals were pretreated with subcutaneous injection (SC) of methyl-scopolamine nitrate (1 mg/kg, Sigma–Aldrich). Then, animals receive an intraperitoneal injection of pilocarpine hydrochloride (360 mg/kg, Sigma–Aldrich) to induce SE. After

90 min of SE onset, seizures were interrupted by SC administration of diazepam (10 mg/kg, União Química). Control animals received a similar volume of sterile saline instead of pilocarpine. Rats were transcardially perfused for brain fixation 48 h after the induction of SE. Perfusion consisted of 0.9% saline solution followed by 1% paraformaldehyde (PFA). The brains were removed, submitted to post-fixation in 1% PFA (at 4°C for 4 h), and dehydrated in 30% sucrose (4 °C) until precipitation. The brains were embedded in cryoprotectant material (OCT) and 12 μm sections were obtained with a cryostat (Leica, CM1860). Section brain tissues were incubated with antibodies against ARC 1:1000 (Synaptic System, cat n°156003) diluted in 0.3% Triton X-100 in phosphate buffer (PB) with 5% normal goat serum (NGS) overnight at room temperature. Next, the sections were incubated with appropriate secondary antibodies conjugated to Alexa 488 (Invitrogen) in PB containing 0.3% Triton X-100 with 3% NGS for 2 h. Counterstaining of brain sections was achieved using 4',6-diamidino-2-phenylindole (DAPI), diluted in the secondary antibody solution. Controls for the experiments consisted of the omission of primary antibodies. The tissue was analyzed in Leica DM5500B inverted microscope (Leica Microsystems). Figures were mounted with Adobe Photoshop CS5 (Adobe Systems Inc.). Image analyses were performed with ImageJ software (National Institute of Mental Health, Bethesda, Maryland, USA) and NIS elements (Nikon Instruments Inc.), using 24 hippocampal slices (n = 4) for each experiment. For ARC analyses in hippocampal principal cell layers, quantifications of the mean pixel intensity in CA1, CA3, and granular cell layer (GCL) were performed for the control and experimental groups after channel separation (RGB) of color images. We calculated the proportional mean pixel intensity of each area relative to the intensity of the three regions summed, where values correspond to the brightness of the pixels. Values from analyses of both groups were entered into a one-way analysis of variance (ANOVA), followed by pairwise comparisons in Tukey's HSD test, with the significance level set at 5%. To characterize the so-called intense ARC immunoreactive neurons (IAIN), we randomly determined the mean pixel intensity of these cells (≈50 cells) in the three regions where this phenotype was observed (CA1, CA3, and hilus). The intensity values of each image were normalized by its median and clustered by group and region. This data was used to calculate the probability density distribution. For this purpose, the method known as Kernel Density Estimation was applied. This is a non-parametric statistical method to estimate the probability density, used instead of histograms to obtain smoother curves [47]. The probability density distributions were fitted using Gaussian curves to identify different groups of cells regarding their pixel intensities. It was considered the existence of two different populations of cells in the case of the absence of overlap between the curves. The point of intersection between two Gaussian was used as a threshold to identify, count, and compare the number of IAINs in the control and experimental group. Values from analyses were entered into unpaired two-sample t-tests with the significance level set at 5%. All mathematical calculations for these analyses were performed using the software MATLAB and the Curve Fitting Toolbox.

3. Results

It has been shown that networks of adaptive neurons present synchronized bursts when there is an increase in excitatory coupling [12] and/or a decrease in inhibitory coupling [10] in networks with random connectivity. Here, we first explored what happens when only 10% of the neurons (only IAINs) have changes in their synaptic input. Fig. 3 compares the network dynamics when all cells have the same excitatory conductance (Fig. 3(a-d)) with the activity pattern when IAINs have an increase in 50% the excitatory conductance $g_{\mathrm{IAIN}} = 1.5$ (Fig. 3 (e-h)). Fig. 3(a) and 3(e) show the raster plot of the neuronal network. In these figures, the spike of each neuron i is represented by a green dot on the time axis. Fig. 3(b) and 3(f) show three examples of the membrane potential of the dynamics shown in the raster plots. Fig. 3(c) and 3(g) show the instantaneous order parameter (red line) and the instantaneous coefficient of variation (blue line). The time interval shown in Fig. 3(a-c) and 3(e-g) correspond to interval identified with a green square dash line in Fig. 3(d) and 3(h), respectively.

The control case shows all neurons firing in the spike asynchronous pattern characterized by CV$<$ 0.5 and R$<$ 0.75 (Fig. 3(a-d)), this is similar to physiological states, where most neurons show the spike pattern. However, for the case where IAINs have stronger connections (Fig. 3(e-h)), burst synchronization is observed with CV$>$ 0.5 and R$>$ 0.75, this exacerbated synchronization is related with epileptic seizure. Therefore, when we increased the incoming excitatory synaptic weight of IAINs from $g^{\mathrm{ex}}_{\mathrm{IAIN}} = 0.5$ nS to $g^{\mathrm{ex}}_{\mathrm{IAIN}} = 0.75$ nS the firing pattern changed from asynchronous to burst synchronization.

Epileptic seizures lasted from a few seconds to a few minutes. A firing pattern similar to the physiological state was observed between crises in epileptic animals. Therefore, to simulate the behavior of an animal with chronic epilepsy for a long time, it was necessary to model an intermittent behavior between the two firing patterns. For some parameters of our model, this was observed. Fig. 4(a) shows the instantaneous order parameter (red line) and the coefficient of variation (blue line) for intermittent activity in the neuronal network. As shown in Fig. 4(a), such activity was characterized by states of asynchronous spikes and synchronous burst activities. We associated these two activities with the up (synchronous bursts) and down states (asynchronous spikes). Unlike the activity that occurs under anesthesia and sleep states, here we have up and down states with firing frequency related to epileptic seizures. In our model, during the synchronous burst pattern, the instantaneous mean firing frequency reaches values above 10 Hz (Fig. 3(e)), consistent with ripples observed in epilepsy [48]. Note that, $R(t)$ and $CV(t)$ are distinct diagnostics associated with synchronization and firing patterns (spike or burst), respectively. However, in this model, such diagnostics are correlated in time. Fig. 4(b) shows a magnification of $R(t)$ and $CV(t)$ time series, for the time around 400 s, indicated by the dashed green square in Fig. 4(a). Each time period of synchronized bursting activity was characterized by the symbol τ.

We explored the parameter space $f_{\mathrm{IAIN}} \times g_{\mathrm{IAIN}}$ to find the values where intermittent activity was observed. Fig. 4(c) shows the mean coefficient of variation for the neuronal network varying f_{IAIN} and g_{IAIN}. The increase of both fractions of IAINs and conductance associated with IAINs contributed to the appearance of burst firing patterns. The parameter region where $\overline{\mathrm{CV}} < 0.5$ presented asynchronous states, while $\overline{\mathrm{CV}} > 0.7$ only synchronous bursts were presented. In the transition, however, a mix of both up and down states could be found for $\overline{\mathrm{CV}} \approx 0.6$. Fig. 4(d) shows the up states number (n_{up}) in the parameter space, in the color region where intermittent activity is observed.

In order to better characterize these transitions, we fixed f_{IAIN} and explored g_{IAIN} in a small range. Fig. 4(e) shows the mean order parameter and coefficient of variation as a function of g_{IAIN} for a fixed f_{IAIN}=0.1. The mean of these two diagnostics, beyond the instantaneous one, were also strongly correlated. In the intermittency case, each up state period, k, was characterized by a τ_k. Fig. 4(f) shows the number of up states (n_{up}) and the total up period (T_{up}), which was considered as the sum of all τ's values, namely $T_{\mathrm{up}} = \sum_k \tau_k$. An optimal value of g_{IAIN} generates the bigger n_{up} value and increasing g_{IAIN} generates an enlargement of the total time of up states T_{up}.

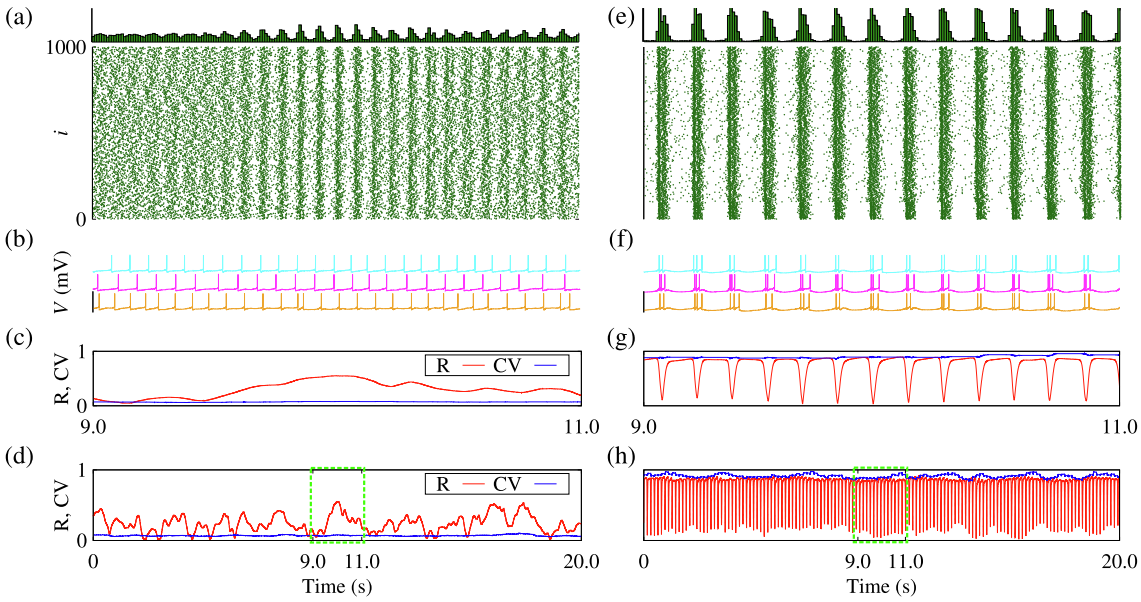

Fig. 3. Comparison of the dynamical behavior between $g_{IAIN} = 1.0$, in (a-d), and $g_{IAIN} = 1.5$, in (e-h). Figures (a) and (e) display the raster plot with a spike histogram above, the vertical bar corresponding to 50 spikes per second and bin width of 10 s was considered. In (b) and (f) the curves show the potential membrane in the function of time, the interval for each curve is 100 mV. (c) and (g) display the order parameter R, in red curves, and the CV in blue curves. These curves are the amplification of the region delimited by the dashed green rectangle in (d) and (h).

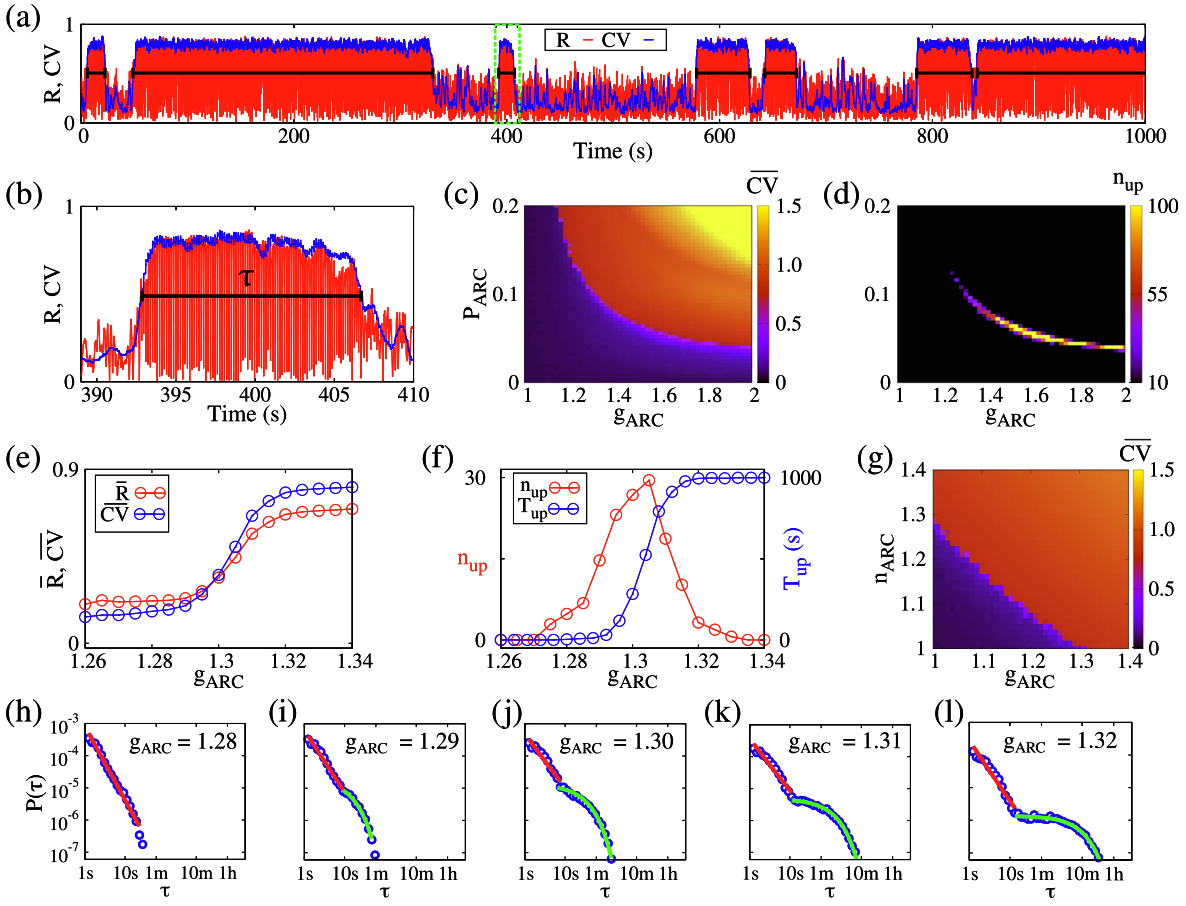

Fig. 4. Intermittent dynamic activity is found in the neuronal network. In (a) the red curve shows the order parameter R, and the blue curve shows the CV overtime, with $g_{IAIN} = 1.31$. The region delimited by the green rectangle is amplified in (b), where $\tau \approx 16$ s. In (c) and (d), the dependence of $\overline{CV}$ and n_{up} with f_{IAIN} and g_{IAIN} are shown in color scale, respectively. (e) $\bar{R}$ (red) and $\overline{CV}$ (blue) in function of g_{IAIN}. (f) n_{up} (red) and T_{up} (blue) in function of g_{IAIN}. (g) $\overline{CV}$ in function of n_{IAIN} and g_{IAIN} in color scale. (h-l) Distribution of τ (blue circles) in logarithmic scale. The red and green curves are power-law and exponential fit, respectively. In (a-b) and (e-l) $f_{IAIN} = 0.1$.

To model the increase in IAIN connectivity, we varied the number of afferent synapses. All neurons have connection probability $p = 0.1$ when the ratio of IAIN and non-IAIN afferent synapse numbers n_{IAIN}=1. When n_{IAIN}=1.4 the afferent connection probability for IAINs neurons are 40% bigger. Fig. 4(g) shows the mean coefficient of variation as a function of g_{IAIN} and n_{IAIN}. The ratio of IAIN and non-IAIN together with the increase of g_{IAIN} also leads the neuron dynamics to show burst activity. The effect of both parameters in the alteration of the firing pattern is very similar in our model.

The period of each synchronized bursting activity (up state) τ might be related to the duration of an epileptic seizure. Therefore, it is possible to relate the severity of epilepsy by looking at the τ values in simulations with long time duration. Fig. 4(h-l) show the τ distribution considering different values of g_{IAIN}, namely (h) g_{IAIN}= 1.28, (i) g_{IAIN}= 1.29, (j) g_{IAIN}= 1.30, (k) g_{IAIN}= 1.31, and (l) g_{IAIN}= 1.32. We observed that for g_{IAIN}= 1.28, τ periods were lower than 30 s, it could become larger as 1 min period for g_{IAIN}=1.29 (Fig. 4(i)). Comparing these two cases it was also possible to note that the first one was more related to a power-law distribution than the second one. This distancing of the power-law fit becomes more evident with the g_{IAIN} increase. In Fig. 4(h-l) the power-law adjusts to become less pronounced for high g_{IAIN}. The coefficients obtained from the power-law fit (Fig. 4(h-l)) can be used as a rule for future predictions in addition to simulations. For the result adjusted in Fig. 4(h) the coefficient was -2.27 while in Fig. 4(l) was -1.84. In Fig. 4(j), (k), and (l), it is also notable that larger periods of up states are found by the neuronal dynamics. Moreover, for τ larger than 10 s the probability is given by $P(\tau) \propto \exp(-k\tau)$ in Fig. 4(i-l), with k equal to $9.4 \times 10^{-2}, 3.5 \times 10^{-2}, 0.9 \times 10^{-2}$, and 0.19×10^{-2}, respectively. $P(\tau)$ is progressively going towards higher values for $\tau > 1$ min, it was observed $P(\tau) > 10^{-7}$ in Fig. 4(i-l), and for $\tau > 10$ min $P(\tau) > 10^{-7}$ only in Fig. 4(l). In Table 2, we show the fitted coefficients of the Fig. 4(h-l) (red and green lines).

To deepen the understanding of the influence of IAINs and non-IAINs in the synchronized burst control, we investigated how the application of yellow and blue light in non-IAINs and IAINs could have a role to suppress the high synchronous activities in the intermittent regimes. While yellow light generated a reduction in neuron excitability, blue one increased the firing rate of the target cells. The effect of light on the neurons was taken into account considering a negative and positive current as of the effect of yellow and blue light. To simulate a very non-invasive situation, we considered that only 1% of neurons were transfected and became photosensitive. Our main objective was to verify whether light stimuli have more effect on IANIs than on non-IANIs.

First, we considered the application of optogenetics control in non-IAINs. Fig. 5(a-f) shows an attempt to suppress intermittent activity using the optogenetics method applied in the non-IAINs of the network. Fig. 5(a) shows three membrane potentials of non-IAINs, the first one without photosensitivity, the second and third with yellow photosensitivity. Fig. 5(b) shows the raster plot for part of the neuronal network (i=[700,900]) where it is possible

Table 2
Curve fits of the probability related to the Fig. 4(h-l). In the red lines $P(\tau) = A\ \tau^{-\gamma}$ while $P(\tau) = B \times \exp(-k\tau)$ in the green lines. The coefficients (A, γ, B, k) were fitted considering τ in seconds.

Fig. 4	A	γ	B	k
(h)	8.24×10^{-4}	2.27		
(i)	6.16×10^{-4}	1.92	1.9×10^{-5}	9.4×10^{-2}
(j)	4.85×10^{-4}	1.67	1.3×10^{-5}	3.5×10^{-2}
(k)	3.60×10^{-4}	1.62	0.47×10^{-5}	0.9×10^{-2}
(l)	2.74×10^{-4}	1.84	0.14×10^{-5}	0.19×10^{-2}

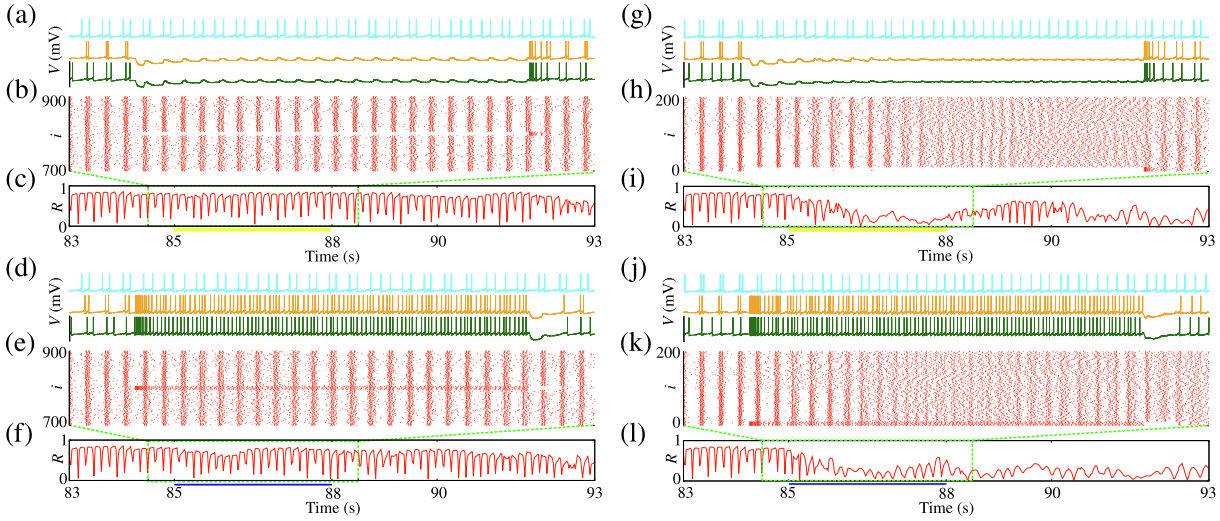

Fig. 5. Simulation of optogenetics methods to suppress the synchronized bursting activity (up states). (a-c) Reduction of excitability and silencing of non-IAINs by application of yellow light. (d-f) Increase of excitability and increasing the firing rate of non-IAINs by application of blue light. In (a-c) 1% of neurons were inhibited for 3 s (yellow light on). In (d-f) the same cell amount was excited for 3 s (blue light on). The membrane potentials are exhibited in (a) and (d). The Cyan curve is from a non-photosensible cell, while the orange and green are from photosensible cells. Figures (b) and (e) show the raster plot for 200 neurons with the 20 photosensible in the middle. The range time is delimited by the green rectangle. A curve in (c) and (f) shows the R in the function of time. The yellow and blue lines indicate the period when the light was on. (g-l) are the same as (a-f) but considering that the 10 photosensible neurons were IAINs. $f_{IAIN} = 0.1$ and $g_{IAIN} = 1.30$ for all simulations.

to observe the neurons which are silent due to yellow light. Fig. 5 (a) and (b) represent the time windows of the instantaneous order parameter shown in Fig. 5(c). The time period that yellow light was on (3 s) is represented by a yellow bar in Fig. 5(c). As can be noticed in Fig. 5(b) and (c), during and after the yellow light application any significant modification in the firing pattern and synchronization of all the neuronal networks was observed.

Since the previous approach did not control the high synchronization, we considered the increase of non-IAIN excitability. Fig. 5(d) shows three membrane potentials of non-IAINs, the first one without photosensitivity, the second and third with photosensitivity due to blue light. Fig. 5(b) shows the raster plot for part of the neuronal network (i=[700,900]) where it is possible to observe higher firing rate neurons due to the application of blue light. Fig. 5 (d) and (e) represent the time windows of the instantaneous order parameter shown in Fig. 5(f). The time period that blue light was on (3 s) is represented by a blue bar in Fig. 5(f). Similarly to the yellow light, the blue one application did not generate any significant modification in the firing pattern and synchronization of all the neuronal networks.

We finally considered the application of optogenetics control in IAINs. Fig. 5(g-l) shows the application of yellow and blue light in IAINs. Fig. 5(g) three membrane potentials of IAIN neurons, the first one without photosensitivity (cyan curve), the second (orange curve), and the third (green curve) with yellow light photosensitivity. Fig. 5(h) shows the raster plot for part of the neuronal network (i=[1]) where it is possible to observe silent neurons due to yellow light. Significant modification in the firing pattern and synchronization of all the neuronal networks was observed during and after the yellow application. The instantaneous order parameter decreased even after the light was turned off (Fig. 5(i)). The same effect was observed for the blue light in IAINs (Fig. 5(j-l)). Therefore, the light application led the network dynamics from synchronous to asynchronous activity when IANIs were chosen to be photosensitive.

4. Conclusion

In this work, we considered a random network composed of excitatory and inhibitory neurons, where the individual neuronal dynamics were described by the adaptive exponential integrate-and-fire model. This neuronal model is capable of exhibiting both spikes and burst-firing activities. After status epilepticus, excitatory neurons can be identified as non-IAINs or IAINs. In the considered model, initially, all neurons were randomly connected with the same probability, then only the excitatory connections received by the IAINs were changed. IAINs may have a higher probability and strength of received excitatory connections, while inhibitory connections between non-IAINs were not altered. This modification in the excitatory connections can participate in epileptogenesis.

We observed that the increase in fraction and synaptic conductance of excitatory IAINs improved the emergence of synchronized burst firing. Besides that, favor the appearance of intermittent behaviors on the synchronization and firing patterns in a neuronal network that did not exhibit this pronounced activity. Such intermittent behavior between synchronous bursts and asynchronous spikes was associated with up and down states of activity. Since intermittent synchronization can be related to epileptic activities, we utilized the instantaneous coefficient of variation to monitor the intermittency of spike and burst patterns along the time. The intermittency of the firing pattern is also related to synchronous and asynchronous activities of the network. For weak increases in IAINs conductance, we observed an approximate power-law distribution of the up states periods. As the IAINs conductance increased, we observed the intermittency behavior in two distinct time scales of burst synchronized activities (up states). Power-law adjustments were made from the distribution of the up states periods, the values of the coefficients obtained can be used in a rule for future prediction in addition to simulations. For the conductance of weak IAINs the angular coefficient was -2.27 while for the strong IAINs the conductance was -1.84, showing that longer events are more likely to happen in the latter case. Moreover, in the distribution of events larger than 10s exponential fit was observed with strong IAINs, however, the probabilities of the events occurring were less than 10^{-4}. The duration of up states depended on the excitatory conductance of IAINs. Therefore, the connections received by IAINs are directly related to the onset of epileptic seizures.

As a method of controlling the high synchronous burst (up states), we simulated the application of optogenetics on non-IAINs and IAINs in the intermittent activities, more specifically during up states. In non-IAINs, both the reduction and increase of excitability by yellow and blue light did not lead the neuron dynamics to asynchronous activity. Otherwise, in IAINs, such application of both yellow and blue light exhibited a strong influence on the network dynamics to return for asynchronous spikes. These results point to the importance of IAINs for high synchronous activity generation and control using optogenetics methods. Taken together, our results revealed that neurons that have more synapses than average (IAINs) may constitute a therapeutic target for the treatment of epileptic seizures.

Declaration of Competing Interest

The authors declare that the research was conducted in the absence of any commercial or financial relationships that could be construed as a potential conflict of interest.

Acknowledgements

This study was possible by partial financial support from the following Brazilian government agencies: CNPq (433782/2016-1), CAPES, and FAPESP (2011/19296-1, 2015/07311-7, 2016/16148-5, 2017/18977-1, 2019/17892-8, 2019/15024-9, 2020/04624-2, 2022/09277-4, and 2022/13761-9).

References

[1] Fisher RS, WvE Boas, Blume W, Elger C, Genton P, Lee P, et al. Epileptic Seizures and Epilepsy: Definitions Proposed by the International League Against Epilepsy (ILAE) and the International Bureau for Epilepsy (IBE). Epilepsia 2015;46:470–2.
[2] Fisher RS, Scharfman HE, deCurtis M. How can we identify ictal and interictal abnormal activity? In: Scharfman HE, Buckmaster PS, editors. Issues in clinical epileptology: A view from the bench, advances in experimental medicine and biology 813. Springer Science+Business Media Dordrecht; 2014.
[3] Barone V, van Putten MJAM, Visser GH. Absence epilepsy: Characteristics, pathophysiology, attention impairments, and the related risk of accidents. A narrative review. Epilepsy Behav 2020;112:107342.
[4] Goetz CG. Textbook of clinical neurology. third ed. Elsevier Inc; 2007.
[5] Theodore WH, Porter RJ, Albert P, Kelley K, Bromfield E, Devinsky O, et al. The secondarily generalized tonic-clonic seizure. Am Acad Neurol 1994;44:1401–7.
[6] Trinka E, Höfler J, Zerbs A. Causes of status epileticus. Epilepsia 2012;53:124–38.
[7] Dobesberger J, Ristic AJ, Walser G, Kuchukhidze G, Unterberger I, Hofle J, et al. Duration of focal complex, secondarily generalized tonic–clonic, and primarily generalized tonic–clonic seizures — A video-EEG analysis. Epilepsy Behav 2015;49:111–7.
[8] Jenssen S, Gracely EJ, Sperling MR. How long do most seizures last? A systematic comparison of seizures recorded in the epilepsy monitoring unit. Epilepsy 2006;47(9):1499–503.
[9] Protachevicz PR, Borges RR, Reis AS, Borges FS, Iarosz KC, Caldas IL, et al. Synchronous behaviour in network model based on human cortico-cortical connections. Physiol Meas 2018;39:074006.

[10] Protachevicz PR, Borges FS, Lameu EL, Ji P, Iarosz KC, Kihara AH, et al. Bistable firing pattern in a neural network model. Front Comput Neurosci 2019;13:19.
[11] Kinjo ER, Higa GSV, Morya E, Valle AC, Kihara AH, Britto LRG. Reciprocal regulation of epileptiform neuronal oscillations and electrical synapses in the rat hippocampus. Plos One 2014;9:e109149.
[12] Borges FS, Protachevicz PR, Lameu EL, Bonetti RC, Iarosz KC, Caldas IL, et al. Synchronised firing patterns in a random network of adaptive exponential integrate-and-fire neuron model. Neural Networks 2017;90:1–7.
[13] Kinjo ER, Rodrıguez PXR, dos Santos BA, Higa GSV, Ferraz MSA, Schemeltzer C, et al. New insights on temporal lobe epilepsy based on plasticity-related network changes and high-order statistics. Mol Neurobiol 2018;55:3990–8.
[14] Morgan RJ, Soltesz I. Nonrandom connectivity of the epileptic dentate gyrys predicts a major role for neuronal hubs in seizures. Proc Nat Acad Sci 2008;105:6179–84.
[15] Bassi SM, Iezzi E, Gilio L, Centonze D, Buttari F. Synaptic plasticity shapes brain connectivity: implications for network topology. Int J Mol Sci 2019;20 (24):6193.
[16] National Institute of Neurological Disorders and Stroke. The Epilepsies and Seizures: Hope Through Research, https://www.ninds.nih.gov/health-information/patient-caregiver-education/hope-through-research/epilepsies-and-seizures-hope-through-research; 2015 [accessed 22 November 2022].
[17] Janz P, Hauser P, Heining K, Nestel S, Kirsch M, Egertm U, et al. Position- and time-dependent Arc expression links neuronal activity to synaptic plasticity during epileptogenesis. Front Cell Neurosci 2018;12:244.
[18] Zhang H, Bramham CR. Arc/Arg3.1 function in long-term synaptic plasticity: Emerging mechanisms and unresolved issues. Eur J Neurosci 2020;54 (8):6696–712.
[19] Yu S, Wang G, Yao B, Xiao L, Tuo H. Arc and Homer1 are involved in comorbid epilepsy and depression: A microarray data analysis. Epilepsy Behav 2022;132:108738.
[20] Rodriguez PXR. Regulation of synaptic and plasticity-related proteins by ryanodine receptors during epileptogenesis. Dissertation, São Bernardo do Campo; 2016.
[21] Ren M, Cao V, Ye Y, Manji HK, Wang KH. Arc regulates experience-dependent persistent firing patterns in frontal cortex. J Neurosci 2014;34:6583–95.
[22] Hattiangady B, Rao MS, Shetty AK. Chronic temporal lobe epilepsy is associated with severely declined dentade neurogenesis in adult hippocampus. Neurobiol Dis 2004;17:473–90.
[23] Vazdarjanova A, Ramirez-Amaya V, Insel N, Plummer TK, Rosi S, Chowdhury S, et al. Spatial exploration induces ARC, a plasticity-related immediate-early gene, only in calcium/calmodulin-dependent protein kinase II-positive principal excitatory and inhibitory neurons of the rat forebrain. J Comparat Neurol 2006;498:317–9.
[24] Acharya MN, Hattiangady B, Shetty AK. Progress in neuroprotective strategies for preventing epilepsy. Progress Neurobiol 2018;84:363–404.
[25] Burman RJ, Raimondo JV, Jefferys JGR, Sen A. Akerman CJ The transition to status epilepticus: how the brain meets the demands of perpetual seizure activity. Seizure: Eur J Epileps 2020;75:137–44.
[26] Hauptmann C, Gail A, Giannakopoulos F. Intermittent burst synchronization in neural networks. Computational Methods in Neural Modeling. IWANN 2003. Lecture Notes in Computer Science, 2686, Springer, Berlin, Heidelberg, 2003.
[27] Koronovskii AA, Hramov AE, Grubov VV, Moskalenko OI, Sitnikova E, Pavlov AN. Coexistence of intermittencies in the neuronal network of epileptic brain. Phys Rev E 2016;2016(93):0322220.
[28] Koloskova AD, Moskalenko OI. Determining the degree of synchronization for intermittent phase synchronization in human electroencephalography data. Tech Phys Lett 2017;43:499–502.
[29] Liu H, Zhang P. Phase synchronization dynamics of neural network during seizures. Comput Mathe Methods Med. Hindawi 2018:1354915.
[30] Moskalenko OI, Koloskova AD, Zhuravlev MO, Koronovskii AA, Hramov AE. Intermittent phase synchronization in human epileptic brain. Proc. SPIE 10063, Dynamics and Fluctuations in Biomedical Photonics XIV 2017;1006316.
[31] Joshi J, Rubart M, Zhu W. Optogenetics: background, methodology advances and potential applications for cardiovascular research and medicine. Front Bioengen Biotecnol 2020;7:466.
[32] Paz JT, Huguenard JR. Optogenetics and epilepsy: past, present and future: shedding light on seizure mechanisms and potential treatments. Epilepsy Currents 2015;15:34–8.
[33] Pourbadie HG, Sayyah M. Optogenetics: control of brain using light. Iranian Biomed J 2018;22(1):4–5.
[34] Mohanty SK, Lakshminarayananan V. Optical techniques in optogenetics. J Mod Opt 2015;62:949–70.
[35] Spagnuolo GM, Genovese F, Fortunato L, Simeone M, Rengo C, Tatullo M. The impact of optogenetics on regenerative medicine. Appl Sci 2020;10:173.
[36] Tonnesen J, Sorensen AT, Deisseroth K, Lundberg C, Kokaia M. Optognetics control of epileptiform activity. Proc Nat Acad Sci 2009;105(29):12162–7.
[37] Krook-Magnuson E, Armstrong C, Oijala M, Soltesz I. On-demand optogenetic control of spontaneous seizures in temporal lobe epilepsy. Nat Comun 2012;4:1376.
[38] Wykes RC, Heeroma JH, Mantoan L, Zheng K, MacDonald DC, Deisseroth K, et al. Optogenetic and potassium channel gene therapy in a rodent model of focal neocortical epilepsy. Sci Transl Med 2013;4(161):161ra152.
[39] Wykes RC, Kullmann DM, Pavlov I, Magloire V. Optogenetics approaches to treat epilepsy. J Neurosci Methods 2016;260:215–20.
[40] Erdös P, Rényi A. On random graphs, I. Publ Mathe 1959;6:290–7.
[41] Brette R, Gerstner W. Adaptive exponential integrate-and-fire model as an effective description of neuronal activity. J Neurophysiol 2005;94:3637–42.
[42] Borges FS, Protachevicz PR, Pena RFO, Lameu EL, Higa GSV, Kihara AH, et al. Self-sustained activity of low firing rate in balanced networks. Phys A 2020;537:122671.
[43] Santos MS, Protachevicz PR, Iarosz KC, Caldas IL, Viana RL, Borges FS, et al. Spike-burst chimera states in an adaptive exponential integrate-and-fire neuronal network. Chaos 2019;29:043106.
[44] Brunel N. Dynamics of networks of randomly connected excitatory and inhibitory spiking neurons. J Physiol 2000;94:445–63.
[45] Ostojic S. Two types of asynchronous activity in networks of excitatory and inhibitory spiking neurons. Nat Neurosci 2014;17(4):594–600.
[46] Chawla MK, Gray DT, Nguyen C, Dhaliwal H, Zempare M, Okuno H, et al. Seizure-Induced Arc mRNA expression thresholds in rat hippocampus and perirhinal cortex. Front Cell Neurosci 2018;12:53.
[47] Botev ZI, Grotowski JF, Kroese DP. Kernel density estimation via diffusion. Ann Stat 2010;38:2916–57.
[48] Malerba P, Krishnan GP, Fellous J-M, Bazhenov M. Hippocampal CA1 ripples as inhibitory transients. PLoS Comput Biol 2016;12(4):e1004880.
[49] Protachevicz PR, Borges FS, Iarosz KC, Baptista MS, Lameu EL, Hansen M, et al. Influence of delayed conductance on neuronal synchronization. Front Physiol 2020;11:1053.
[50] Borges FS, Protachevicz PR, Santos V, Santos MS, Gabrick EC, Iarosz KC, et al. Influence of inhibitory synapses on the criticality of excitable neuronal networks. Indian Acad Sci Conf Ser 2020;3:97–103.
[51] Naud R, Marcille N, Clopath C, Gerstner W. Firing patterns in the adaptive exponential integrate-and-fire model. Biol Cybern 2008;99:335–47.
[52] Badel L, Lefort S, Brette R, Petersen CCH, Gerstner W, Richardson MJE. Dynamic IV curves are reliable predictors of naturalistic pyramidal-neuron voltage traces. Am Physiol Soc 2008;99:656–66.
[53] Clopath C, Jolivet R, Rauch A, Lüscher HR, Gerstner W. Predicting neuronal activity with simple models of the threshold type: Adaptive Exponential Integrate-and-Fire model with two compartments. Neurocomputing 2007;70:1668–73.
[54] Gabbiani F, Koch C. Principles of spike train analysis. In: Koch C, Segev I, editors. Methods in neuronal modeling: from ions to networks. Cambridge, MA: MIT Press; 1998. p. 313–60.
[55] Protachevicz PR, Santos MS, Seifert EG, Gabrick EC, Borges FS, Borges RR, et al. Noise induces continuous and noncontinuous transitions in neuronal interspike intervals range. Indian Acad Sci Conf Ser 2020;3:105–9.
[56] Kuramoto Y. Chemical oscillations, waves, and turbulence. Berlin: Springer-Verlag; 1984.